JGR Oceans

RESEARCH ARTICLE
10.1029/2018JC014695

Tide Gauge Records Show That the 18.61-Year Nodal Tidal Cycle Can Change High Water Levels by up to 30 cm

Dongju Peng[1], Emma M. Hill[1,2], Aron J. Meltzner[1,2], and Adam D. Switzer[1,2]

[1]Earth Observatory of Singapore, Nanyang Technological University, Singapore, [2]Asian School of Environment, Nanyang Technological University, Singapore

Key Points:
- We find that nodal modulations have the largest influences at locations in the Gulf of Tonkin, English Channel and Bristol Channel
- We demonstrate that nodal modulation in the diurnal and semidiurnal locations will peak again in 2025 and 2034, respectively
- We identify several locations within close proximity to one another where the 18.61-year nodal cycle is out of phase

Supporting Information:
- Supporting Information S1

Correspondence to:
D. Peng,
djpeng@ntu.edu.sg

Citation:
Peng, D., Hill, E. M., Meltzner, A. J., & Switzer, A. D. (2019). Tide gauge records show that the 18.61-year nodal tidal cycle can change high water levels by up to 30 cm. *Journal of Geophysical Research: Oceans*, *124*, 736–749. https://doi.org/10.1029/2018JC014695

Received 18 OCT 2018
Accepted 7 JAN 2019
Accepted article online 10 JAN 2019
Published online 29 JAN 2019

Abstract The lunar nodal cycle, produced by the varying declination of the Moon over a period of 18.61 years, drives changes in tidal amplitude globally. However, constraining the range of changes in tidal amplitude that can be expected over a nodal cycle from real observations is rarely considered for coastal hazard planning. In this study, we use hourly tide gauge observations with record lengths >19 years from 574 stations distributed worldwide to examine the contribution of the nodal modulation to monthly high water levels. Our results show that the influence of the lunar nodal cycle on high water levels is largest at tide gauge stations located in the Gulf of Tonkin, English Channel, and Bristol Channel, amounting up to 30 cm in range, suggesting that in the coming decades the impact of the nodal cycle on high water levels in those regions could be greater than that of global mean sea level rise, which is up to 17 cm by 2030, according to the Intergovernmental Panel on Climate Change fifth assessment report projections. We also examine the phase of nodal modulation and show that the estimated phases exhibit two clusters: one cluster ($111° \pm 10°$) corresponds with the locations having a diurnal form of tides, whereas the other cluster ($-59° \pm 11°$) corresponds with the locations exhibiting a semidiurnal form of tides. Nodal modulation in the diurnal and semidiurnal locations will peak again in 2025 and 2034, respectively, resulting in enhanced potential for coastal hazard in the respective regions.

Plain Language Summary Nodal modulation is slow variation of the amplitude of diurnal or semidiurnal ocean tides associated with relative motions of the Earth, Moon, and Sun over a period of 18.61 years. It is an important contributor to extreme sea levels and can increase the risk of coastal flooding at specific, forecastable times. We use hourly tide gauge observations from 574 stations distributed worldwide to estimate and map the contribution of the 18.61-year lunar nodal modulation to monthly high water levels. We find that nodal modulation has the largest influence on the monthly highest water levels at locations in the Gulf of Tonkin, in the Bristol Channel, and in the English Channel, amounting up to 30 cm in range, and the nodal modulation in the diurnal and semidiurnal locations will peak again in 2025 and 2034, respectively, with the potential for high levels of coastal hazard in the respective regions.

1. Introduction

Coastal flooding caused by extreme sea levels is a major concern for low-lying and highly populated coastal areas (Church et al., 2007; Li, Switzer, et al., 2018; Neumann et al., 2015; Stocker, 2014). Mean sea level (MSL), episodic water level fluctuations due to climate extremes, and astronomical tides all affect total observed sea levels and contribute to the occurrence of extreme high water levels. With the popular interest in increased risk of flood events in a future warmer climate, most studies have focused on the effects of climate extremes (storm surges) and MSL changes (Cazenave et al., 2018; Herring et al., 2015; Kay et al., 2015; Muis et al., 2016; Nicholls & Cazenave, 2010; Zhang & Sheng, 2015); these studies suggested that extreme sea levels have been increasing during the past few decades at many locations around the world, and a large part of the increase can be accounted for by changes in MSL rather than changes in the frequency and magnitude of storm surges.

Astronomical tides—the rise and fall of sea levels caused by the combined effects of the gravitational forces exerted by the Moon and the Sun on a rotating Earth—have a significant influence on coastal water levels. Astronomical tides are regular and recurring, but when a high tide coincides with a storm surge, it can threaten coastal communities and the consequences can be devastating. Historically, many disastrous coastal floods have been caused by the coincidence of large meteorologically induced surges and large or even moderately high astronomical tides (Table 12.5; Pugh & Woodworth, 2014). As a recent example, Super Typhoon

Hato (23 August 2017) coincided with moderately high astronomical tides (0.9 m above MSL), resulting in storm tides (a combination of astronomical tides and storm surge) reaching up to 2.8 and 2.4 m (above MSL) in Zhuhai and Hong Kong (Hong Kong Observatory, 2017) and causing widespread flooding in the coastal areas around the Pearl River Estuary in southern China. Twenty-four fatalities, 845 injuries, and 6.82 billion USD direct economic losses were reported (Economic and Social Commission for Asia and the Pacific/World Meteorological Organization Typhoon Committee, 2017). The peak astronomical tide in August 2017 for that region was 1.3 m above MSL. Li, Yang, et al. (2018) reproduced the entire Typhoon Hato event using the tide-surge-wave coupled hydrodynamic model—Semiimplicit Cross-scale Hydroscience Integrated System Mode—together with the Weather Research and Forecasting Model and demonstrated that flooding would have been more severe if Typhoon Hato had occurred at higher astronomical tidal levels.

The lunar nodal cycle, produced by the varying declination of the Moon over a period of 18.61 years, is the main tidal force influencing high tides on decadal timescales (Pugh & Woodworth, 2014); it drives changes in tidal amplitude globally, affecting coastal habitat formation, shoreline landforms, and salt marsh vegetation (Berger et al., 2004; Gratiot et al., 2008; Yndestad et al., 2008). The evidence for nodal tidal components affecting extreme sea levels has been identified along the coasts of China, Australia, and the United States (Eliot, 2010; X. Feng, Tsimplis, & Woodworth, 2015; Haigh et al., 2010; Shaw & Tsimplis, 2010; Wahl & Chambers, 2015). Eliot (2010) demonstrated that a 7-cm rise in water levels represents a threefold variation in the relative likelihood of extreme flood events at Fremantle, Australia, suggesting that nodal modulation is a significant contributor to extreme sea levels.

Haigh et al. (2011) used modeled tides from the TPXO7.2 global tidal model to assess the influence of the 18.61-year lunar nodal cycle and the 8.85-year cycle of lunar perigee on high tidal levels on a one-quarter degree global grid. However, their study was conducted under two assumptions: (1) the modeled tidal constituents are accurate, and (2) the real nodal tidal constituents conform in the same way as their equilibrium counterparts. Challenging these assumptions, a recent study compared the observed tidal modulations from tide gauge records with their corresponding nodal equilibrium tidal constituents, showing that differences do occur at locations on a shallow continental shelf (X. Feng, Tsimplis, & Woodworth, 2015). In addition, analyzing 16-year satellite altimetry data in the Pacific and the western Atlantic Oceans, Cherniawsky et al. (2010) found that the observed nodal amplitude ratios between $(O_{1n}, K_{1n}, M_{2n}, K_{2n})$ and (O_1, K_1, M_2, K_2) tend to exceed the values predicted by equilibrium tidal theory.

Tidal features in coastal areas, especially those on shallow continental shelves, vary greatly from one site to another as both water depth and shoreline geometry can affect local tides, making the observed 18.61-year lunar nodal modulation different from their astronomically theoretical values. Therefore, constraining the range of changes in tidal amplitude that can be expected over a nodal cycle from real observations is valuable for coastal hazard planning. To the best of our knowledge, only Menéndez and Woodworth (2010) used real data to detect the 18.61-year lunar nodal cycle at a global scale; however, their nodal findings were obtained from only two cycles of data in the records commencing in 1970, and this was not the focus of their study. In this study, we use a global tide gauge data set to examine the influence of the 18.61-year lunar nodal modulation on different high water levels with the aim to estimate decadal changes in tidal amplitude and to provide predictions of periods where there is enhanced risk of flooding to coastal infrastructure. We first extract monthly time series of different high water levels from the hourly tide gauge records for each station and apply a 12-month moving median filter. We then model the 18.61-year lunar nodal modulation from the filtered time series using harmonic analysis. Lastly, we map the range and phase of the 18.61-year lunar nodal modulation and identify locations where they most influence high water levels.

2. Data and Methods

2.1. Sea-Level Data Sets

We obtained high-frequency tide gauge records from the Global Extreme Sea Level Analysis Version 2 (GESLA-2, http://www.gesla.org/) and the University of Hawaii Sea Level Center (UHSLC, https://uhslc.soest.hawaii.edu/). The GESLA-2 data set contains research quality sea-level information from 1,355 stations distributed worldwide (Woodworth et al., 2017). UHSLC regularly collects, processes, analyzes, and distributes tide gauge observations from nearly 700 stations and 88 international agencies in support of climate

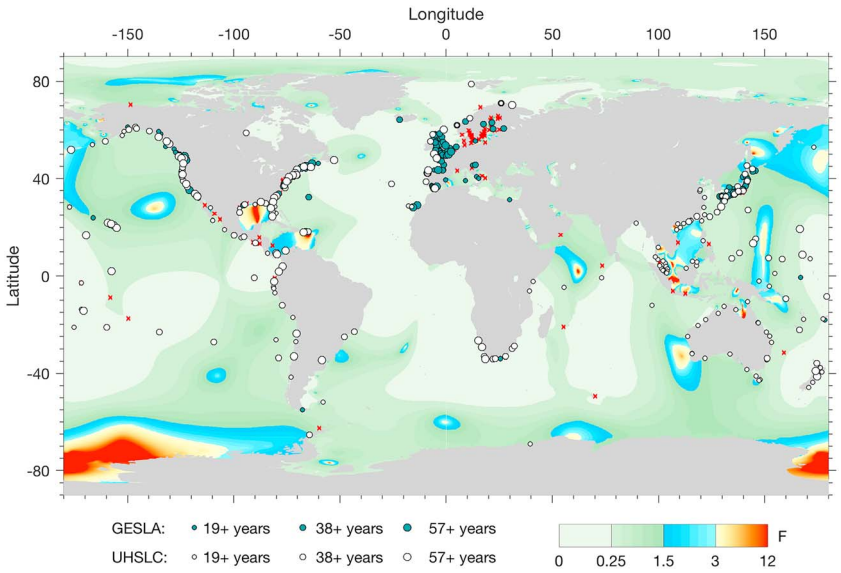

Figure 1. Distribution of tide gauge stations used for analysis of the 18.61-year lunar nodal cycle and the corresponding record lengths. Circles represent tide gauge stations where the 18.61-year nodal cycle is identified using our techniques; red crosses indicate tide gauge stations where we are not able to detect the 18.61-year nodal cycle in the three selected high water levels, although they meet our criteria of data selection. Color map represents tidal form factor, which is defined by the ratio of the amplitudes of the two main diurnal and semidiurnal constituents (K_1,O_1, M_2, and S_2), $F = (H_{K_1} + H_{O_1})/(H_{M_2} + H_{S_2})$. The amplitudes used to make this map were taken from the Oregon State University TPXO8-atlas global tide model, http://volkov.oce.orst.edu/tides/tpxo8_atlas.html. Tidal forms are classified as follows: $0 < F < 0.25$, semidiurnal; $0.25 < F < 1.5$, mixed and mainly semidiurnal; $1.5 < F < 3.0$, mixed and mainly diurnal; and $F > 3.0$, diurnal. GESLA = Global Extreme Sea Level Analysis; UHSLC = University of Hawaii Sea Level Center.

and oceanographic research (Caldwell et al., 2015) and is one of the main data sources of the GESLA-2 data set. Sea-level information from both GESLA-2 and UHSLC are at hourly or greater frequencies. As the GESLA-2 data set has not been updated since March 2017, we replaced the tide gauge records in the GESLA-2 data set originating from UHSLC with the up-to-date research quality sea-level data that we directly obtained from UHSLC. In this study, we standardized the use of hourly values, which make up the majority of the two data sets, by subsampling any available higher-frequency data. This will mean that in some cases high percentile water levels are slightly underestimated.

Raw tide gauge records include contributions from MSL, astronomical tides, meteorologically and oceanographically induced water level changes, vertical land movements, systematic bias, and noise; identification of the 18.61-year lunar nodal signals therefore requires suitable data sets and dedicated analysis techniques. Tide gauge observations from 574 stations meet our criteria of data selection (described in section 2.2), and significant influence of the 18.61-year lunar nodal modulation on the three selected high water levels is detected at 478 stations using our techniques (described in sections 2.3 and 2.4). Geographic locations of the tide gauge stations are shown in Figure 1. Among the 478 stations, 231 are from GESLA-2 (91, 98, and 42 stations with record lengths >19, >38, and >57 years, respectively), and 247 are from UHSLC (106, 77, and 64 stations with record lengths >19, >38, and >57 years, respectively).

2.2. Data Selection

We select data based on record lengths and data completeness. Stations with record lengths <19 years are discarded to ensure that at least one full oscillation of the 18.61-year lunar nodal cycle is captured. In order to detect nodal signals from as many stations as possible, we did not standardize the use of record lengths in nodal modulation modeling (described in section 2.4). The record lengths we used are thus varied, with the longest records being from 1846 to 2017 at Brest, France. We transform the raw hourly records to monthly values to model the 18.61-year lunar nodal cycle (described in section 2.3) and assess data completeness based on the monthly time series. Generally, we select stations where data completeness is >70% for further analysis. However, for some stations with record lengths >38 years, data completeness still meets our criteria even though the data contain a large data gap (>9 years). To ensure that nodal modulation modeling would

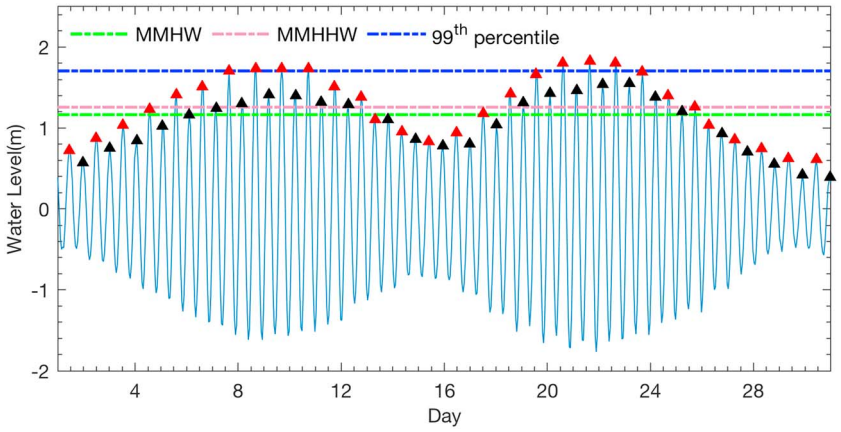

Figure 2. A demonstration of the three high water levels (MMHW, MMHHW, and the 99th percentile) at a location with tides in semidiurnal form. Red and black triangles represent higher-high waters and lower-high waters, respectively. MMHW = monthly mean high waters; MMHHW = monthly mean higher-high waters.

not be biased or corrupted by such a large data gap, we adopt a detect-locate-trim approach to preprocess the monthly time series. We first perform a data gap detection. Once large data gap is identified, we then locate the gap in the monthly time series. Lastly, we trim the time series according to the location of the gap. If the gap is located in the middle of the time series and the record lengths of the data in front of and behind the gap are >19 years, we do not make any changes to this type of time series, but if the gap is located at the head or tail of the time series and the record lengths of the data either in front of or behind the gap is <9 years, we trim the time series by removing the large gap together with the data in front of or behind the gap with record lengths <9 years. Record lengths shown in Figure 1 are based on the trimmed data.

2.3. Data Preprocessing

Analyses of time series at different percentile water levels and analyses of monthly or annual mean high water levels have been extensively used in extreme sea level studies (Haigh et al., 2010; Marcos et al., 2015; Menéndez & Woodworth, 2010; Wahl et al., 2017; Woodworth & Blackman, 2004). In this study, we choose to calculate the following three types of time series to characterize the 18.61-year lunar nodal cycle and estimate its contribution to different high water levels: (1) the monthly 99th percentile water level, (2) monthly mean high waters (MMHW), an average level of all high water levels, and (3) monthly mean higher-high waters (MMHHW), an average level of the higher-high waters. For the first type of time series, to consider the sensitivity of the results to the percentile level chosen, we also calculated for each station the time series for an additional eight percentile water levels (80th, 90th, 95th, 98th, 99.5th, 99.8th, and 99.9th percentiles and monthly maxima).

As an example, Figure 2 shows hourly tide gauge records at a station with semidiurnal tides over a month. The three types of high water levels for that month are illustrated with dash lines in green, pink, and blue. A month (31 days) with no data gaps contains 744 hourly measurements; these values are ordered in terms of height and then used to compute the 99th percentile level and the additional eight percentile levels. MMHW for this station is calculated as the average of higher-high waters (red triangles) and lower-high waters (black triangles). Due to shallow water distortions at some locations—especially where tidal range is small (< 1 m)—four high tides a day occur (Pugh & Woodworth, 2014); in this case, calculation of MMHW is based on the daily four high water levels. MMHHW for this station is calculated as the average of red triangles shown in Figure 2. For locations with tides in diurnal form, MMHW and MMHHW, are identical. We show examples of the three types of time series at the four selected stations representing the four tidal forms in Figure S1 in the supporting information.

It has been demonstrated that analysis of extreme sea levels based on annual calculations could be corrupted if a small number of incorrectly measured hourly values occur around high waters (Menéndez & Woodworth, 2010). In this study, we first extract the three types of monthly time series from the hourly tide gauge records and subtract the monthly median (the 50th percentile) of the hourly values to remove the

effect of MSL changes. Gaps summing to more than 30% of the hourly values for a given month invalidate the use of this monthly value. Second, we apply a 12-month moving median filter to the monthly time series. An advantage of the filtered monthly calculations over raw annual calculations is that occasional data errors are less likely to strongly bias the filtered monthly calculations. Figure S2 in the supporting information shows four representative monthly time series with and without the 12-month moving median filter applied and nodal modulations estimated from the corresponding filtered and nonfiltered time series, demonstrating that this simple filtering technique significantly improves the quality of data for lunar nodal cycle modeling.

2.4. Nodal Modulation Model

We estimate the amplitude and phase of the 18.61-year lunar nodal modulation using least squares and the filtered monthly time series. Our model includes a harmonic function with a period of 18.61 years, a period of 4.4 years, a linear trend, and a constant. The expression is as follows:

$$H(t) = \beta_0 + \beta_1(t) + \beta_2\cos(\omega_1 t) + \beta_3\sin(\omega_1 t) + \beta_4\cos(\omega_2 t) + \beta_5\sin(\omega_2 t) + \varepsilon \quad (1)$$

$$\omega_1 = \frac{2\pi}{18.61}, \omega_2 = \frac{2\pi}{4.4}$$

where $H(t)$ is the monthly value at time t, t is the time in units of year, β_0 is the constant value, β_1 is the linear trend, and β_2 and β_3 are the amplitudes of the cosine and sine functions of the 18.61-year lunar nodal modulation. β_4 and β_5 are the amplitudes of the cosine and sine functions of the 4.4-year modulation, and ε is noise.

Evidence for an increase in annual mean high water relative to MSL has been reported at locations in the English Channel, along the Iberian Atlantic coast, and along the coastlines of the United States and China (J. Feng, von Storch, et al., 2015; Fortunato et al., 2016; Haigh et al., 2010; Wahl & Chambers, 2015). In addition, the 8.85-year cycle of lunar perigee affects high tidal levels as a quasi 4.4-year cycle, and its influence on high tidal levels has also been identified (Haigh et al., 2011; Menéndez & Woodworth, 2010).

To ensure that the linear trend and the 4.4-year modulation do not affect the estimation of the 18.61-year modulation, we first estimate all the parameters in equation (1); if the linear trend and the 4.4-year modulation are relatively significant (amplitude of the 4.4-year modulation >1 cm or > 40% of the 18.61-year modulation amplitude), we remove the two effects and reconstruct a new time series $H'(t)$ to reestimate β_2 and β_3. The amplitude A and phase φ of the 18.61-year lunar nodal modulation are derived as below

$$H'(t) = \beta_2\cos(\omega_1 t) + \beta_3\sin(\omega_1 t) + \varepsilon \quad (2)$$

$$A = \sqrt{\beta_2^2 + \beta_3^2}; \varphi = \tan^{-1}\left(\frac{\beta_3}{\beta_2}\right) \quad (3)$$

We consider the result of the least squares fitting to be significant when the amplitude of the estimated nodal modulation is greater than the corresponding root mean square of the residuals, and the percentage of the total variance explained by the regression model (R squared) is greater than 50%. R squared (R^2), also known as the coefficient of determination, is a statistical measure of how close the data are to the fitted regression model.

3. Results

3.1. Comparison of Percentile, MMHW, and MMHHW Time Series

Analysis of the monthly time series without removing the 4.4-year modulation at the nine selected percentile water levels for each station reveals that the influence of the 4.4-year modulation of lunar perigee is negligible at low percentile levels (<99th). Figure 3 shows the nine monthly time series from a location with tides in semidiurnal form, indicating that at this station the 4.4-year modulation dominates the 18.61-year modulation at high percentile water levels, and the effect of the 4.4-year modulation at low percentile water levels is negligible.

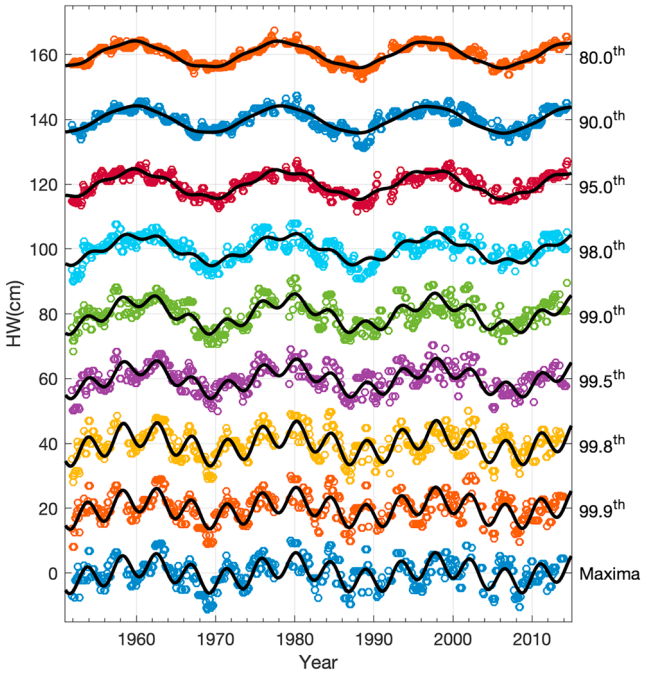

Figure 3. A demonstration of the dominant 4.4-year modulation in the high percentile water levels. Hourly tide gauge records are from a station located at Tumaco, Colombia (01°49′ N,78°44′ W). The form factor at this station is 0.09, and the tidal range is 3.0 m. HW = high waters.

Examining the monthly time series without the effect of the 4.4-year modulation at the nine selected percentile water levels for each station, we find that when lower percentiles are considered, the range (twice amplitude) of the 18.61-year lunar nodal modulation is reduced. In contrast, the coefficient of determination of the least squares fitting is increased, indicating that the time series at lower percentile levels better fit the nodal modulation model. Figure 4 shows the range of the 18.61-year lunar nodal modulation estimated from the monthly time series for a location in Canada, at the nine selected percentile water levels, with the linear trend and the 4.4-year modulation removed (the nine monthly time series are shown Figure S2 in the supporting information). Figure 4 also shows the corresponding coefficients of determination of the least squares fitting. Together, these demonstrate that the amplitudes of the 18.61-year lunar nodal modulation on high water levels are sensitive to the percentile level chosen.

Removal of the monthly median (50th percentile) in the high water levels chosen subtracts much of the seasonal and interannual variability that is responsible for changes in MSL. However, high water levels can also include meteorologically induced sea level changes and other nontidal signals that are not represented in the MSL time series: these signals make the extraction of the nodal signals more difficult and could corrupt the estimation of the 18.61-year nodal modulation. Among the 574 stations that meet our criteria of data selections, 207, 253, and 371 stations are identified with significant nodal signals in the monthly 99.9th, 99th, and 90th percentile time series, respectively, suggesting that the higher the percentile water level chosen, the more likely the nodal signals are contaminated. Distributions of those stations are shown in Figure 11 in section 3.2 and Figures S7 and S11 in the supporting information.

To quantify the changes in range when choosing a different percentile, we compare the ranges of the 18.61-year lunar nodal modulation estimated from the monthly time series at the 99.9th, 99th and 90th percentile water levels (Figure 5). Taking the nodal modulations estimated from the monthly 99.9th percentile time series as a reference, the ranges of the nodal modulation are reduced by ~10% and ~30%, when the 99th and 90th percentile water levels are chosen. We understand that the 18.61-year lunar nodal modulation in the 99.9th percentile or monthly maximum water level is more practical. However, considering that the range of the 18.61-year lunar nodal modulation estimated from the 99th percentile time series is not substantially reduced compared with those from the 99.9th percentile times series and there are more stations where the nodal signals are not significantly contaminated by other forcing factors, we thus select the 99th percentile water level for discussion in the subsequent sections.

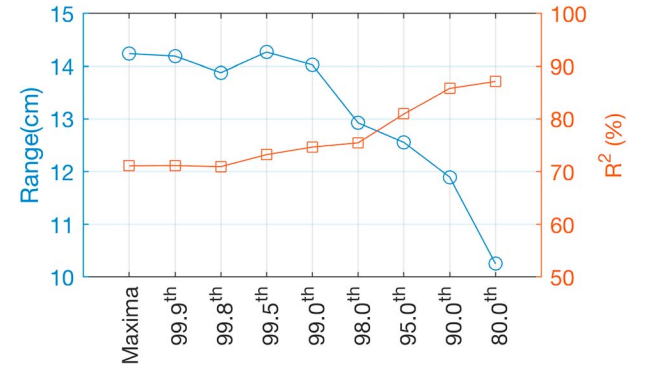

Figure 4. Range of nodal modulation and *R* squared of the least squares fitting plotted against percentiles for a station located at Victoria, Canada (40°26′ N,123°22′ W). The form factor at this station is 2.11, and the tidal range is 2.8 m.

The effect of the 4.4-year modulation in the MMHW and MMHHW time series is negligible as well (not shown), thus allowing focus on the 18.61-year lunar nodal modulation. A comparison of the 99th percentile, MMHHW, and MMHW time series at four sites that represent the four tidal forms, semidiurnal, mixed and mainly semidiurnal, mixed and mainly diurnal, and diurnal, is shown in Figure S1 in the supporting information. An analysis of the coefficient of determination reveals that among the 99th percentile, MMHHW, and MMHW time series, MMHW is the one that best fits the nodal modulation model in all forms of tides; among the 574 stations, there are 253, 417, and 423 stations with the coefficient of determination >50% in the least squares fitting of the nodal modulation model and the 99th percentile, MMHHW, and MMHW time series, respectively. In addition, the ranges of the 18.61-year lunar nodal modulation in the 99th percentile, MMHHW, and MMHW time series for each

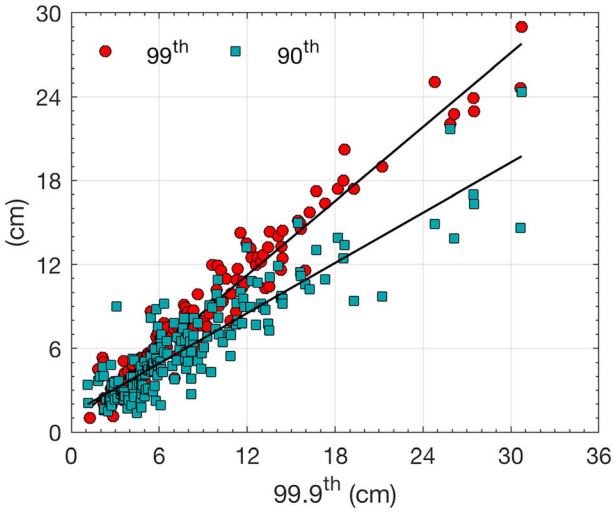

Figure 5. Ranges of the nodal modulation estimated from the 99th and 90th percentile time series plotted against that from the 99.9th percentile time series. The black line is a linear fit of the ranges from the 99.9th and 99th percentile time series and from the 99.9th and 90th percentile time series.

station vary with tidal form. Generally, the range of the nodal modulation is largest for the 99th percentile time series, and it is the smallest for the MMHHW time series. Figure 6 shows the ranges of the nodal modulation in the MMHW and MMHHW time series, plotted against the ranges for the 99th percentile water levels. For locations with $F < 1.5$, which make up ~90% of the data set, the difference between the ranges of the nodal modulation in the 99th percentile water level and MMHW is statistically insignificant, while the ranges of the nodal modulation in the MMHHW are reduced by ~10% compared to those from the 99th percentile time series.

Although not a focus of this study, we compare the influences of the 4.4-year and the 18.61-year modulations on the monthly maximum water levels and find that the amplitude of the 4.4-year modulation is larger than the 18.61-year modulation amplitude at 52 stations, suggesting that at these locations the 4.4-year modulation dominates the 18.61-year modulation in the monthly maximum water levels. These stations are located on Peninsular Malaysia (along the east coast facing the South China Sea and the west coast facing the Malacca Strait), in the Bay of Biscay, in the English Channel, in the Gulf of Cadiz, in the Surabaya, in the northeastern Australia, and along the West Coasts of the United States, Africa, Peru, Ecuador, and Colombia. They all exhibit tides in semidiurnal or mixed and mainly semidiurnal form ($F < 1.5$). In addition, the amplitude of the 4.4-year modulation is either >1 cm or reaching >40% of the 18.61-year modulation amplitude at 90 stations: at these locations, we consider the influence of the 4.4-year modulation on the monthly maximum water levels as significant. Figure 7 shows the geographic location of the stations where dominant and significant influence of the 4.4-year modulations is detected in the monthly maxima time series and the corresponding range of the modulation. The 4.4-year modulation is largest at locations in the Bristol Channel and in the English Channel where tidal ranges are >6 m; tidal range for each tide gauge station used in this study is shown in Figure S4 in the supporting information.

3.2. Range of Nodal Modulation

Figure 8 shows the range of the 18.61-year lunar nodal modulation estimated from the MMHW time series. The contribution of the nodal modulation to the MMHW is <10 cm in range at most stations (~86%); strong effect of the 18.61-year lunar nodal cycle on the MMHW (between 10 and 20 cm in range) is found at locations on the northwest Australian Shelf, in the Bay of Fundy, along the west coast of Panama, in the Gulf of Alaska, and along the coastline of southern Chile. The nodal modulation has the largest influence on the

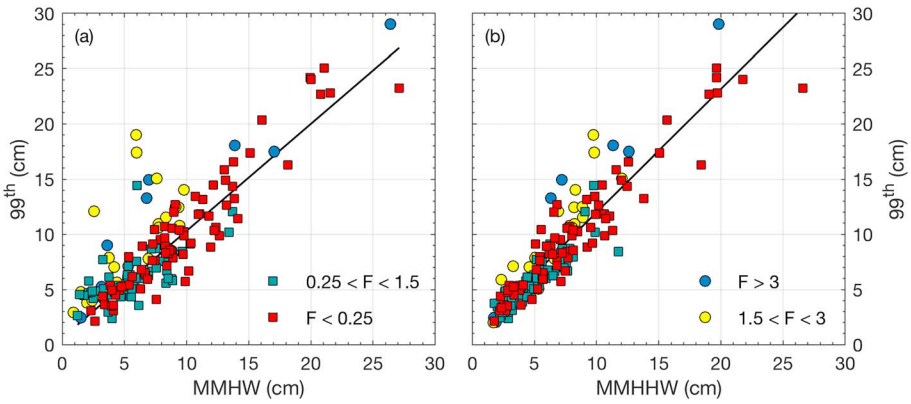

Figure 6. Comparison of ranges of nodal modulations estimated from the 99th percentile time series and the (a) MMHW and (b) MMHHW time series. Colors indicate the form factor of the tides. The black line is a linear fit of the two ranges at locations with $F < 1.5$. MMHW = monthly mean high waters. MMHHW = monthly mean higher-high waters.

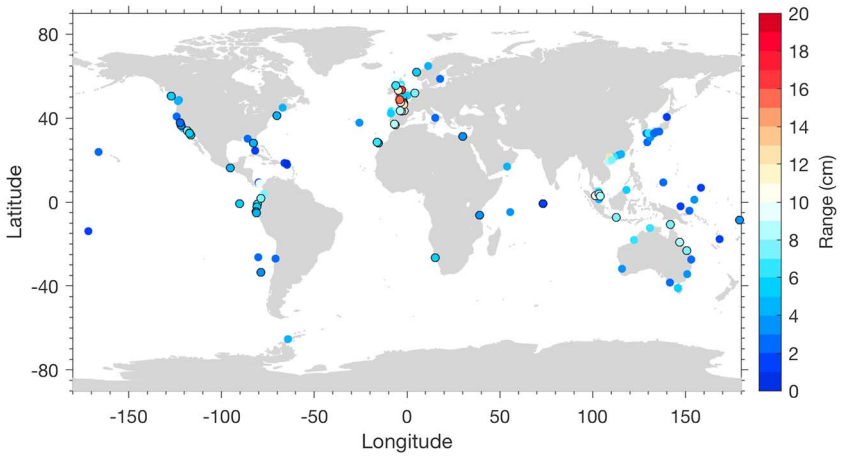

Figure 7. Range of the 4.4-year modulation from the monthly maxima time series. Colored circles with black edge are locations where the 4.4-year modulation dominates the 18.61-year nodal modulation. For comparison, we show the range of the 18.61-year nodal modulations from the monthly maxima time series in Figure S6 in the supporting information. Sites that are not shown in the figure are locations where we are not able to detect the 4.4-year cycle in the monthly maxima time series using the technique described in section 2.4.

MMHW (between 20 and 30 cm in range) at locations in the Gulf of Tonkin, in the Bristol Channel, and in the English Channel.

The range of the nodal modulation is related to both the form of tides and the tidal range. In this study, we use the simplified equation in Haigh et al. (2011) to calculate the tidal range. For locations with tides in semidiurnal form, tidal ranges are estimated as the difference between mean high water springs ($MHWS = H_{M_2} + H_{S_2}$) and mean low water springs ($MLWS = -H_{M_2} - H_{S_2}$), whereas for locations with tides in mixed (including both "mixed and mainly semidiurnal" and "mixed and mainly diurnal") or diurnal form, tidal ranges are estimated as the difference between mean higher-high water) and mean lower-low water ($MLLW = -H_{M_2} - H_{O_1} - H_{K_1}$). We estimate amplitudes of the main semidiurnal and diurnal tidal constituents (H_{M_2}, H_{S_2}, H_{O_1}, and H_{K_1}) for each station using the Utide software package (Codiga, 2011) and hourly tide gauge records. We also base calculation of the form factor for each station on the estimated amplitudes of the main tidal constituents.

Generally, the range of the 18.61-year lunar nodal modulation increases with tidal range (Figure 9). However, it increases more with tidal range for locations dominated by diurnal tides as compared to

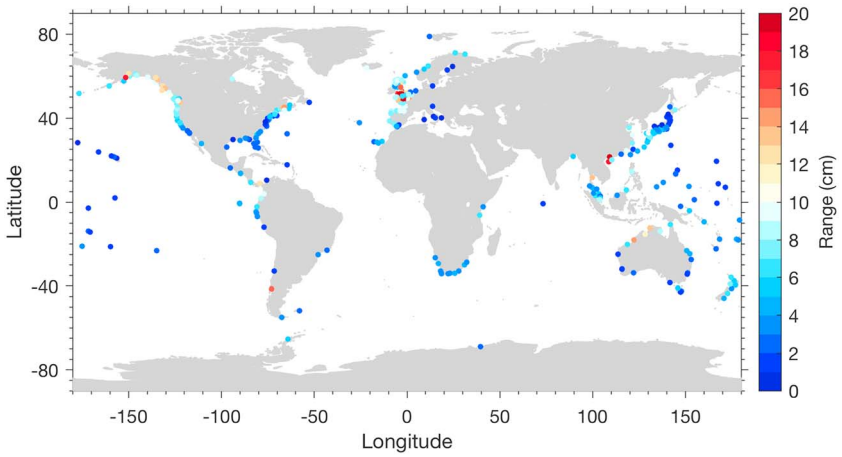

Figure 8. Range of the 18.61-year lunar nodal modulation estimated from the monthly mean high waters time series. Sites that are not shown in the figure are locations where we are not able to detect the 18.61-year lunar nodal cycle in the monthly mean high waters time series using the technique described in section 2.4.

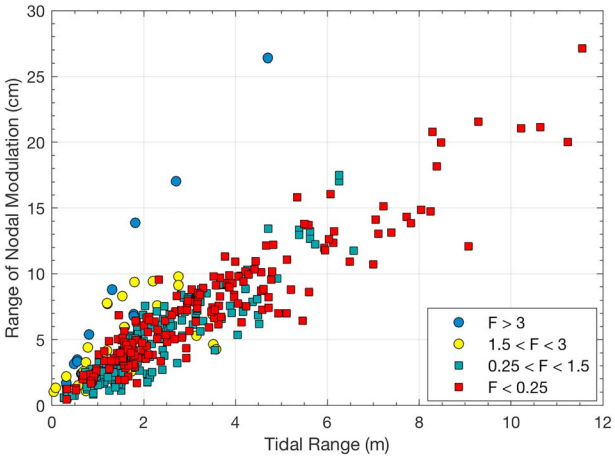

Figure 9. Range of the nodal modulation in the monthly mean high waters plotted against tidal range. The plot distinguishes between stations where the tide is semidiurnal (193 stations), mixed and mainly semidiurnal (184 stations), mixed and mainly diurnal (29 stations), or diurnal (17 stations) in form.

locations dominated by semidiurnal tides. Linear fitting the ranges of the nodal modulation with tidal ranges, the curve of diurnal locations is ~3 times steeper than that of semidiurnal locations. Practically, the range of the nodal modulation is ~6% and ~2% of tidal range at diurnal and semidiurnal locations, respectively. We show the distribution of the ranges of the nodal modulation expressed as a percentage of the corresponding tidal ranges in Figure S5 in the supporting information.

We also calculated the ranges of the 18.61-year lunar nodal modulation from the MMHHW and the nine selected percentile time series. We show the distributions of the ranges of the 18.61-year lunar nodal modulation from the MMHHW and the 99th percentile time series in Figures 10 and 11. For readers who are interested in the ranges of nodal modulation in the additional eight percentiles (monthly maxima, 99.9th, 99.8th, 99.5th, 98th, 95th, 90th, and 80th), the corresponding results are shown in Figures S6 to S13 in the supporting information. We can see from those figures that that the spatial variation of the ranges of the 18.61-year lunar nodal modulation from different types of time series is generally similar, although the range of the 18.61-year lunar nodal modulation is sensitive to the percentile level chosen. In addition, the locations where the nodal modulation has the largest influence are always in the Gulf of Tonkin (located in the South China Sea), in the Bristol Channel, and in the English Channel, no matter which high water level is chosen for assessing the contribution of the 18.61-year nodal modulation. Examining the form factor and the tidal range for each tide gauge station used in this study, we find that the locations in the Bristol Channel and in the English Channel where the nodal modulation is largest are dominated by semidiurnal tides and their tidal ranges are >6 m; The locations in the Gulf of Tonkin are dominated by diurnal tides, and their tidal ranges are between 4 and 6 m, and X. Feng, Tsimplis, and Woodworth (2015) found that compared with other locations in the South China Sea, the locations in the Gulf of Tonkin has the largest amplitudes of the main diurnal constituents O_1 and K_1 (~1 m) as a result of tidal resonance. Therefore, large tidal range and tidal resonance should be responsible for the strong effect of nodal modulation we observed from different levels of high waters in the English and Bristol Channels and in the Gulf of Tonkin.

3.3. Phase of Nodal Modulation

From a coastal flooding prospective, the phase of the nodal modulation is also important as it can increase the risk at specific times. We demonstrated in section 3.1 that compared to the MMHHW time series and the

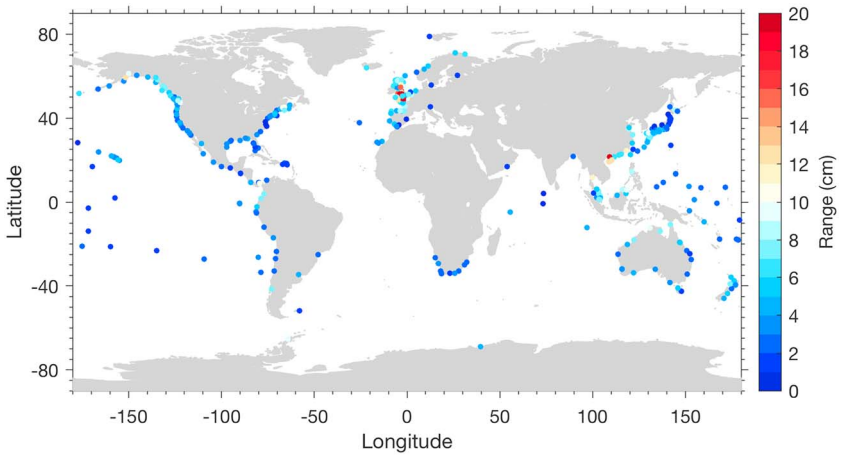

Figure 10. Range of the 18.61-year lunar nodal modulation estimated from the monthly mean higher-high waters time series. Sites that are not shown in the figure are locations where we are not able to detect the 18.61-year lunar nodal cycle in the monthly mean higher-high waters time series using the technique described in section 2.4.

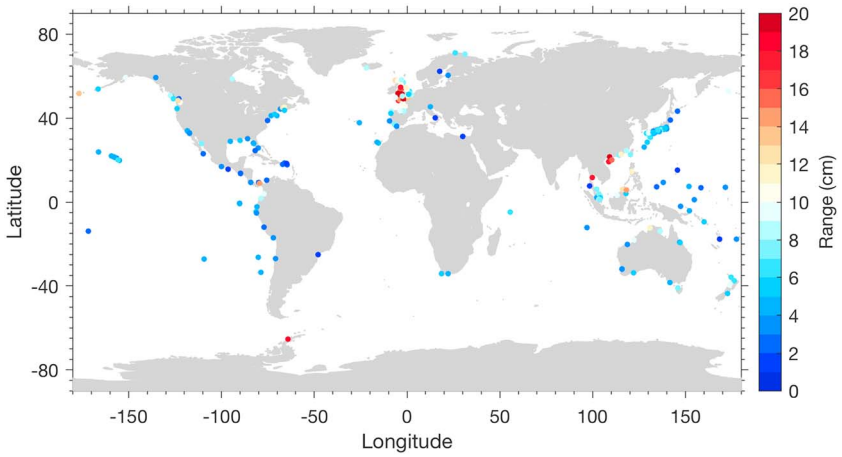

Figure 11. Range of the 18.61-year lunar nodal modulation estimated from the 99th percentile time series. Sites that are not shown in the figure are locations where we are not able to detect the 18.61-year lunar nodal cycle in the 99th percentile time series using the technique described in section 2.4.

nine selected percentile time series, (1) the MMHW time series best fit the nodal modulation model in terms of the coefficient of determination of the least squares fitting, and (2) the MMHW time series are less likely contaminated by other forcing factors; therefore, the number of stations where the 18.61-year lunar nodal signals are successfully identified is the greatest. We thus choose to examine the phase of the nodal modulation in the MMHW time series in this study.

Based on equilibrium tidal theory, when the Moon's declination is at a maximum (28°36′), the nodal modulation of diurnal tides is at a maximum (which last occurred in June 2006), whereas when the Moon's declination is at a minimum (18°18′), the nodal modulation of semidiurnal tides is at a maximum (which last occurred in October 2015). Therefore, the nodal modulation in high water levels should have one of the two phases at a given location depending on whether that location is dominated by semidiurnal or diurnal tides. Figure 12 shows that at two locations where tides are in semidiurnal or mixed and mainly semidiurnal form ($F < 1.5$), the nodal modulation last peaked in 2015, whereas at two locations where tides are in mixed and mainly diurnal or diurnal form ($F > 1.5$), the nodal nodulation last peaked in 2006, consistent with the equilibrium tidal theory.

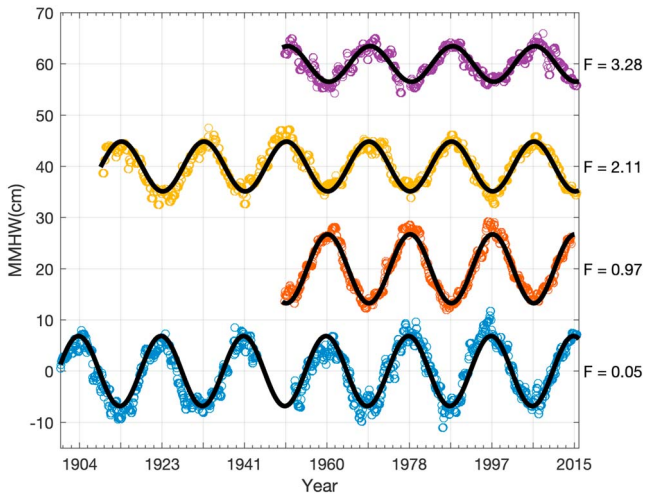

Figure 12. MMHW time series extracted from four locations, representing the four tidal forms. These four stations are located at Brest, France ($F = 0.05$), Seattle, USA ($F = 0.97$), Victoria, Canada ($F = 2.11$), and Alaska, USA ($F = 3.28$). We applied a 12-month moving median filter to the four time series, and only records after 1900 at Brest are shown in the figure. The black line is the nodal cycle modeled from the filtered time series. The numbers in the X axis of the figure are the integer years when the nodal cycle is at peak/nadir. MMHW = monthly mean high waters.

Figure 13 shows the phase of the nodal modulation calculated from the MMHW time series plotted against the form factor. We can see from Figure 13 that the estimated phases exhibit two clusters: one cluster ($111° \pm 10°$) corresponds with the locations where the nodal modulation last peaked in 2006 and correlates with maximum lunar declination, whereas the other cluster ($-59° \pm 11°$) corresponds with the locations where the nodal modulation last peaked in 2015 and correlates with minimum lunar declination. Figure 13 also indicates that the phases of the 18.61-year lunar nodal modulation at locations with tides in mixed and mainly diurnal form ($1.5 < F < 3$) behave like those at locations with diurnal tides ($F > 3.0$). However, for locations with tides in mixed and mainly semidiurnal form ($0.25 < F < 1.5$), the pattern is not as evident as that at locations with tides in mixed and mainly diurnal form: when $0.25 < F < 0.9$, the phases behave like those at locations with semidiurnal tides ($F < 0.25$); when $0.9 < F < 1.5$, the phases at some locations behave like these with semidiurnal tides and the others behave like those with diurnal tides, suggesting the complexity of tidal features and the necessity of constraining the phases of the 18.61-year lunar nodal modulation from real observations.

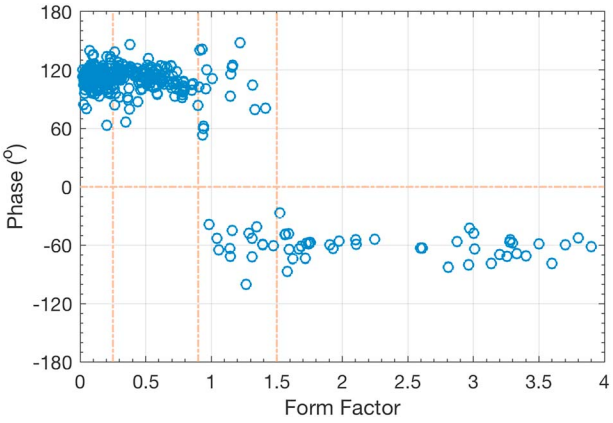

Figure 13. Phase of nodal modulation estimated from the monthly mean high waters time series, plotted against form factor. There are eight stations with form factors >4; for plotting purpose, we reduced those numbers to [3 4] in the figure.

Globally, semidiurnal/diurnal tidal amplitudes increase and decrease at roughly the same time everywhere, but there are significant local differences controlled by the particular bathymetry (open coast vs. inner estuary vs. upriver, etc.) of each tide gauge location. In addition, tidal high water is the maximum tidal level reached during a cycle, but the observed high water level may be greater or less than the predicted tidal level because of meteorological effects. We thus infer that those local factors might be responsible for the variability in the phases of the nodal modulation. Based on the nodal modulation estimated from the filtered MMHW time series, we select two sets of nine locations with the nodal modulation amplitudes ranging from ~2 to ~10 cm to predict the 18.61-year lunar nodal cycle, and the predicted cycles are shown in Figure 14. The two sets of data represent the two clusters of phases, and the two reference times are June 2006 (Figure 14b) and October 2015 (Figure 14a), respectively. Figure 14 shows a clear phase shift in the 18.61-year lunar nodal cycle, particularly for those locations that last peaked in 2006. A shift of 10° in phase means that monthly mean high waters lead or lag the lunar nodal cycle predicted from the equilibrium tidal theory by approximately 6 months.

Figure 15 shows the distribution of the estimated phases from the MMHW time series. Examining Figure 15, we find that the 18.61-year lunar nodal cycle is out of phase at several locations within close proximity to one another. On Peninsular Malaysia, sites along the west coast (facing the Malacca Strait, where tides are semidiurnal) are out of phase with sites along the east coast (facing the South China Sea, where tides are in mixed and mainly semidiurnal form). On the West Coast of North America, there is a phase shift between the Strait of Juan de Fuca (tides in mixed and mainly diurnal form) and the Haro Strait (tides in mixed and mainly semidiurnal form). In Japan, there is a phase shift between the west coast (facing the Sea of Japan) and the east coast (facing the North Pacific Ocean); tides at sites along both the west and east coasts are in mixed and mainly semidiurnal form. In the eastern United States, there is a phase shift between the East Coast (where there are semidiurnal tides) and the coast of the Gulf of Mexico (where there are diurnal tides). In Australia, there is a phase shift between the southern coast (diurnal tides) and northern coast (semidiurnal tides).

4. Discussion

We used hourly tide gauge observations from 574 stations distributed worldwide to estimate the contribution of the 18.61-year lunar nodal modulation to the MMHW, MMHHW, and the monthly 99th percentile water levels with a focus on the MMHW. We understand that the geographical coverage and the number of tide gauge stations used in this study, especially the ones with diurnal tides, is limited; the spatial complexity of the nodal modulation might not be fully captured. In addition, the nodal signals are difficult to separate,

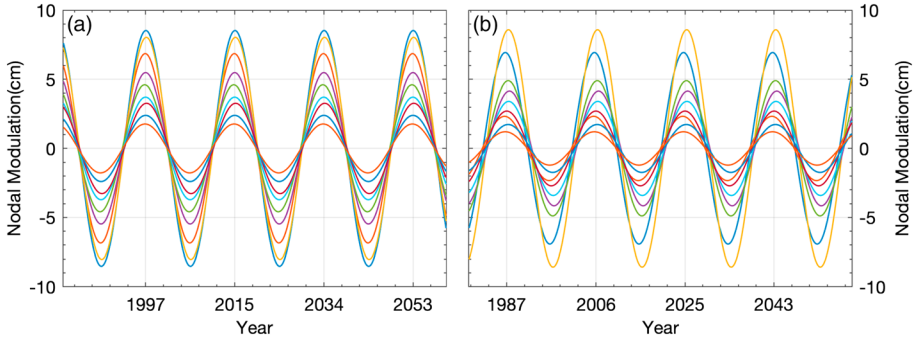

Figure 14. Predicted nodal modulation at the nine selected locations with tides in (a) semidiurnal form and (b) diurnal/mixed and mainly diurnal form. The numbers in the *X* axis of the figures are the integer years when the nodal cycle is at peak.

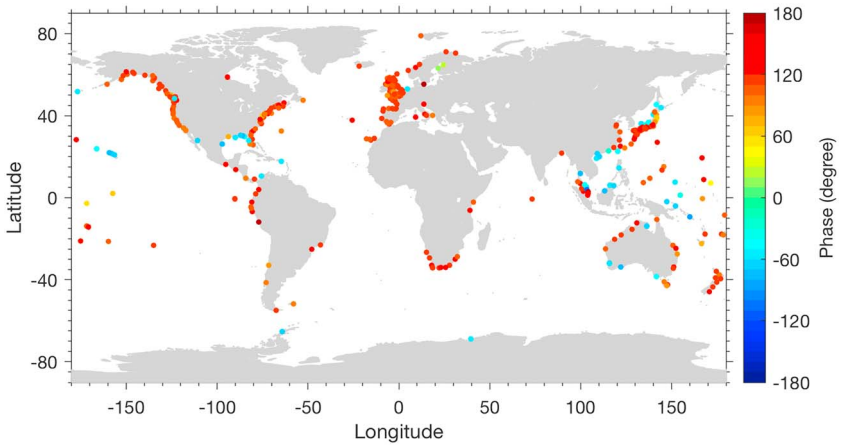

Figure 15. Phase of nodal modulation estimated from the monthly mean high waters time series. Sites that are not shown in the figure are locations where we are not able to detect the 18.61-year lunar nodal cycle in the monthly mean high waters time series using the technique described in section 2.4.

particularly for locations where the tidal ranges are small (<1 m), due to the effects of the meteorologically induced sea-level changes and MSL changes, which may also make the observed high water levels different from tidal high water levels. It is therefore difficult to directly compare our results with those of Haigh et al. (2011). However, the observed patterns generally show good agreement.

Haigh et al. (2011) focused on the influence of the 18.61-year lunar nodal modulation on the annual 99.9th percentile tidal level, whereas our findings are based on the monthly 99th percentile water levels, MMHHW, and MMHW. However, comparing our Figure 9 with Figure 7a in Haigh et al. (2011), both studies show that the amplitude of the 18.61-year lunar nodal modulation generally increases with tidal range, and the effect of nodal modulation is greater for locations dominated by diurnal tides than for locations with same tidal ranges but dominated by semidiurnal tides. In addition, Haigh et al. (2011) found that the 18.61-year lunar nodal modulation is largest in the Gulf of Tonkin, in the Shelikhov Gulf, along the southwestern coast of New Guinea, and in the Ross Sea. Unfortunately, there are no qualified tide gauges in the Shelikhov Gulf, along the coast of New Guinea, and in the Ross Sea, but based on the available coverage of our data set, we identify that the nodal modulation makes the highest contribution at locations in the Gulf of Tonkin, in the English Channel, and in the Bristol Channel. The nodal modulation in the English and Bristol channels was also demonstrated to be large in Haigh et al. (2011) as a result of the large amplitude of the semidiurnal tidal constituents M_{2n} in these regions.

We identify 52 locations showing dominant effects of the 4.4-year modulation of lunar perigee at the monthly highest water levels. Coastal managers in these areas should be aware that enhanced risk of coastal flooding is likely every 4.4 years. In addition, our results indicate that both the 18.61-year lunar nodal modulation and the 4.4-year modulation of lunar perigee are largest in the English Channel and in the Bristol Channel. Compounding this, Leake et al. (2009) demonstrated that surge activity in the English Channel could be potentially increased due to a tendency for storm tracks to move southward by 2077–2099, and MSL along the entire European coastline is projected to rise around 21 and 24 cm by the 2050s under RCP4.5 (Representative Concentration Pathway) and RCP8.5, respectively, to reach 53 and 77 cm by the end of the century (Vousdoukas et al., 2017). The Unite Kingdom has a long history of coastal flooding (Haigh & Nicholls, 2017): changes in MSL, storm surges, and tidal ranges can increase the risk. The unusual sequence of extreme storms and coastal floods over the winter of 2013/2014 is a reminder of the ever-present risks facing coastal communities in the United Kingdom (Huntingford et al., 2014). Therefore, coastal planners must consider all these factors in hazard planning for the region.

Recent studies have demonstrated that the 18.61-year lunar nodal cycle could affect sea-level trends induced by mass redistribution and that it is a necessary component to be considered to close the sea level budget on regional scales (Frederikse et al., 2016; Kleinherenbrink et al., 2017). However, it was assumed in those studies that amplitude of the 18.61-year lunar nodal cycle follows the astronomical equilibrium tidal theory and

no phase shift occurs. Our results, constrained from real observations, could provide useful information in regions where amplitude and phase of the 18.61-year lunar nodal cycle differ from those predicted from the astronomical equilibrium tidal theory.

5. Conclusions

We analyzed hourly tide gauge observations with record lengths >19 years from 574 stations distributed worldwide to map the contribution of the 18.61-year lunar nodal modulation to the MMHW, MMHHW, and monthly 99th percentile water levels. We found that, in some locations, the variability in high water levels from the 18.6-year nodal tidal cycle will be substantially larger than global mean sea-level rise in the next few years to decades. These locations will experience a rise in the highest water level over the next few years that far exceeds global mean sea-level rise. Our results show that the influence of the 18.6-year nodal cycle on high water levels is largest in the Gulf of Tonkin, English Channel, and Bristol Channel, amounting to up to 30 cm in range. In comparison, global mean sea-level rise is projected to rise up to 17 cm by 2030 and to 32 cm by 2050 (Stocker, 2014), according to the Intergovernmental Panel on Climate Change fifth assessment report. Coastal planners should consider for hazard planning these slow variations in high water levels caused by the 18.61-year lunar nodal cycle. We also examined the phase of the nodal modulation in the MMHW, demonstrating that nodal modulation in the diurnal and semidiurnal regions will peak again in 2025 and 2034, respectively, with the potential for high levels of coastal hazard in the respective regions.

Acknowledgments
We are grateful to the Editor Don Chambers and an anonymous reviewer for their suggestions that improved the manuscript. We thank GESLA-2 (http://www.gesla.org/) and UHSLC (https://uhslc.soest.hawaii.edu/) for providing tide gauge data sets. The amplitudes of the tidal constituents for calculating the form factors shown in Figure 1 are derived from the TPXO8-atlas global model (http://volkov.oce.orst.edu/tides/tpxo8_atlas.html). This research was supported by the Singapore Ministry of Education Academic Research Fund Tier 2 (MOE 2016-T2-2-041), by the Earth Observatory of Singapore, the National Research Foundation Singapore, and the Singapore Ministry of Education under the Research Centers of Excellence initiative. This is EOS paper number 207.

References

Berger, W., Schimmelmann, A., & Lange, C. (2004). Tidal cycles in the sediments of Santa Barbara Basin. *Geology*, *32*(4), 329–332. https://doi.org/10.1130/G20249.2

Caldwell, P., Merrifield, M., & Thompson, P. (2015). Sea level measured by tide gauges from the global oceans-the Joint Archive for Sea Level holdings (NCEI Accession 0019568), Version 5.5, NOAA Natl. Centers Environ. Information, Dataset.

Cazenave, A., Palanisamy, H., & Ablain, M. (2018). Contemporary sea level changes from satellite altimetry: What have we learned? What are the new challenges? *Advances in Space Research*, *62*(7), 1639–1653. https://doi.org/10.1016/j.asr.2018.07.017

Cherniawsky, J. Y., Foreman, M. G., Kang, S. K., Scharroo, R., & Eert, A. J. (2010). 18.6-year lunar nodal tides from altimeter data. *Continental Shelf Research*, *30*(6), 575–587. https://doi.org/10.1016/j.csr.2009.10.002

Church, J., Wilson, S., Woodworth, P. L., & Aarup, T. (2007). Understanding sea level rise and variability. *Eos, Transactions American Geophysical Union*, *88*(4), 43–43. https://doi.org/10.1029/2007EO040008

Codiga, D. L. (2011). *Unified tidal analysis and prediction using the UTide Matlab functions*. RI: Graduate School of Oceanography, University of Rhode Island Narragansett.

Eliot, M. (2010). Influence of interannual tidal modulation on coastal flooding along the Western Australian coast. *Journal of Geophysical Research*, *115*, C11013. https://doi.org/10.1029/2010JC006306

Economic and Social Commission for Asia and the Pacific/World Meteorological Organization Typhoon Committee (2017). MEMBER REPORT. Retrieved from http://www.typhooncommittee.org/12IWS/docs/Members/China20171026_final.pdf

Feng, J., von Storch, H., Jiang, W., & Weisse, R. (2015). Assessing changes in extreme sea levels along the coast of China. *Journal of Geophysical Research: Oceans*, *120*, 8039–8051. https://doi.org/10.1002/2015JC011336

Feng, X., Tsimplis, M. N., & Woodworth, P. L. (2015). Nodal variations and long-term changes in the main tides on the coasts of China. *Journal of Geophysical Research: Oceans*, *120*, 1215–1232. https://doi.org/10.1002/2014JC010312

Fortunato, A. B., Li, K., Bertin, X., Rodrigues, M., & Miguez, B. M. (2016). Determination of extreme sea levels along the Iberian Atlantic coast. *Ocean Engineering*, *111*, 471–482. https://doi.org/10.1016/j.oceaneng.2015.11.031

Frederikse, T., Riva, R., Kleinherenbrink, M., Wada, Y., Broeke, M., & Marzeion, B. (2016). Closing the sea level budget on a regional scale: Trends and variability on the Northwestern European continental shelf. *Geophysical Research Letters*, *43*, 10,864–10,872. https://doi.org/10.1002/2016GL070750

Gratiot, N., Anthony, E. J., Gardel, A., Gaucherel, C., Proisy, C., & Wells, J. (2008). Significant contribution of the 18.6 year tidal cycle to regional coastal changes. *Nature Geoscience*, *1*(3), 169–172. https://doi.org/10.1038/ngeo127

Haigh, I., Eliot, M., & Pattiaratchi, C. (2011). Global influences of the 18.61 year nodal cycle and 8.85 year cycle of lunar perigee on high tidal levels. *Journal of Geophysical Research*, *116*, C06025. https://doi.org/10.1029/2010JC006645

Haigh, I. D., & Nicholls, R. J. (2017). Coastal Flooding. *MCCIP Science Review 2017*, 108–114. https://doi.org/10.14465/2017.arc10.009-cof

Haigh, I., Nicholls, R., & Wells, N. (2010). Assessing changes in extreme sea levels: Application to the English Channel, 1900–2006. *Continental Shelf Research*, *30*(9), 1042–1055. https://doi.org/10.1016/j.csr.2010.02.002

Herring, S. C., Hoerling, M. P., Kossin, J. P., Peterson, T. C., & Stott, P. A. (2015). Explaining extreme events of 2014 from a climate perspective. *Bulletin of the American Meteorological Society*, *96*(12), S1–S172.

Hong Kong Observatory (2017). Super Typhoon Hato(1713) Report. Retrieved from http://www.weather.gov.hk/informtc/hato17/report.htm

Huntingford, C., Marsh, T., Scaife, A. A., Kendon, E. J., Hannaford, J., Kay, A. L., et al. (2014). Potential influences on the United Kingdom's floods of winter 2013/14. *Nature Climate Change*, *4*(9), 769–777. https://doi.org/10.1038/nclimate2314

Kay, S., Caesar, J., Wolf, J., Bricheno, L., Nicholls, R., Islam, A. S., et al. (2015). Modelling the increased frequency of extreme sea levels in the Ganges–Brahmaputra–Meghna delta due to sea level rise and other effects of climate change. *Environmental Science: Processes & Impacts*, *17*(7), 1311–1322. https://doi.org/10.1039/c4em00683f

Kleinherenbrink, M., Riva, R., Frederikse, T., Merrifield, M., & Wada, Y. (2017). Trends and interannual variability of mass and steric sea level in the Tropical Asian Seas. *Journal of Geophysical Research: Oceans*, *122*, 6254–6276. https://doi.org/10.1002/2017JC012792

Leake, J., Wolf, J., Lowe, J., Hall, J., & Nicholls, R. (2009). Response of marine climate to future climate change: Application to coastal regions. In *Coastal Engineering 2008: (In 5 Volumes)* (pp. 4354–4364). Singapore: World Scientific.

Li, L., Switzer, A. D., Wang, Y., Chan, C.-H., Qiu, Q., & Weiss, R. (2018). A modest 0.5-m rise in sea level will double the tsunami hazard in Macau. *Science Advances*, *4*(8), eaat1180. https://doi.org/10.1126/sciadv.aat1180

Li, L., Yang, J., Lin, C.-Y., Chua, C. T., Wang, Y., Zhao, K., Wu, Y.-T., et al. (2018). Field survey of Typhoon Hato (2017) and a comparison with storm surge modeling in Macau. *Natural Hazards and Earth System Sciences*, *18*(12), 3167–3178. https://doi.org/10.5194/nhess-18-3167-2018

Marcos, M., Calafat, F. M., Berihuete, Á., & Dangendorf, S. (2015). Long-term variations in global sea level extremes. *Journal of Geophysical Research: Oceans*, *120*, 8115–8134. https://doi.org/10.1002/2015JC011173

Menéndez, M., & Woodworth, P. L. (2010). Changes in extreme high water levels based on a quasi-global tide-gauge data set. *Journal of Geophysical Research*, *115*, C10011. https://doi.org/10.1029/2009JC005997

Muis, S., Verlaan, M., Winsemius, H. C., Aerts, J. C., & Ward, P. J. (2016). A global reanalysis of storm surges and extreme sea levels. *Nature Communications*, *7*(1), 11969. https://doi.org/10.1038/ncomms11969

Neumann, J. E., Emanuel, K., Ravela, S., Ludwig, L., Kirshen, P., Bosma, K., & Martinich, J. (2015). Joint effects of storm surge and sea-level rise on US Coasts: New economic estimates of impacts, adaptation, and benefits of mitigation policy. *Climatic Change*, *129*(1–2), 337–349. https://doi.org/10.1007/s10584-014-1304-z

Nicholls, R. J., & Cazenave, A. (2010). Sea-level rise and its impact on coastal zones. *Science*, *328*(5985), 1517–1520. https://doi.org/10.1126/science.1185782

Pugh, D., & Woodworth, P. L. (2014). *Sea-level science: Understanding tides, surges, tsunamis and mean sea-level changes*. Cambridge: Cambridge University Press. https://doi.org/10.1017/CBO9781139235778

Shaw, A., & Tsimplis, M. (2010). The 18.6 yr nodal modulation in the tides of southern European coasts. *Continental Shelf Research*, *30*(2), 138–151. https://doi.org/10.1016/j.csr.2009.10.006

Stocker, T. (2014). *Climate change 2013: The physical science basis: Working group I contribution to the fifth assessment report of the intergovernmental panel on climate change*. Cambridge: Cambridge University Press.

Vousdoukas, M. I., Mentaschi, L., Voukouvalas, E., Verlaan, M., & Feyen, L. (2017). Extreme sea levels on the rise along Europe's coasts. *Earth's Future*, *5*, 304–323. https://doi.org/10.1002/2016EF000505

Wahl, T., & Chambers, D. P. (2015). Evidence for multidecadal variability in US extreme sea level records. *Journal of Geophysical Research: Oceans*, *120*, 1527–1544. https://doi.org/10.1002/2014JC010443

Wahl, T., Haigh, I., Nicholls, R., Arns, A., Dangendorf, S., Hinkel, J., & Slangen, A. (2017). Understanding extreme sea levels for broad-scale coastal impact and adaptation analysis. *Nature Communications*, *8*, 16075. https://doi.org/10.1038/ncomms16075

Woodworth, P. L., & Blackman, D. L. (2004). Evidence for systematic changes in extreme high waters since the mid-1970s. *Journal of Climate*, *17*(6), 1190–1197. https://doi.org/10.1175/1520-0442(2004)017<1190:EFSCIE>2.0.CO;2

Woodworth, P. L., Hunter, J., Marcos, M., Caldwell, P., Menendez, M., & Haigh, I. (2017). Towards a global higher-frequency sea level dataset. *Geoscience Data Journal*, *3*(2), 50–59.

Yndestad, H., Turrell, W. R., & Ozhigin, V. (2008). Lunar nodal tide effects on variability of sea level, temperature, and salinity in the Faroe-Shetland Channel and the Barents Sea. *Deep Sea Research Part I: Oceanographic Research Papers*, *55*(10), 1201–1217. https://doi.org/10.1016/j.dsr.2008.06.003

Zhang, H., & Sheng, J. (2015). Examination of extreme sea levels due to storm surges and tides over the northwest Pacific Ocean. *Continental Shelf Research*, *93*, 81–97. https://doi.org/10.1016/j.csr.2014.12.001